

Onset of η -meson binding in the He isotopes

N. Barnea, E. Friedman, A. Gal*

Racah Institute of Physics, The Hebrew University, 91904 Jerusalem, Israel

Abstract

The onset of binding $\eta(548)$ mesons in nuclei is studied in the He isotopes by doing precise ηNNN and $\eta NNNN$ few-body stochastic variational method calculations for two semi-realistic NN potentials and two energy dependent ηN potentials derived from coupled-channel models of the $N^*(1535)$ nucleon resonance. The energy dependence of the ηN subthreshold input is treated self consistently. It is found that a minimal value of the real part of the ηN scattering length $a_{\eta N}$ close to 1 fm is required to bind η mesons in ${}^3\text{He}$, yielding then a few MeV η binding in ${}^4\text{He}$. The onset of η -meson binding in ${}^4\text{He}$ requires that $\text{Re} a_{\eta N}$ exceeds 0.7 fm approximately. These results compare well with results of recent ηNNN and $\eta NNNN$ pionless effective field theory calculations. Related optical-model calculations are also discussed.

Keywords: few-body systems, mesic nuclei

1. Introduction

The near-threshold ηN system, where $E_{\text{th}}(\eta N) = 1487$ MeV, couples strongly to the nearby $N^*(1535)$ resonance, resulting in a fairly attractive and weakly absorptive energy dependent s -wave ηN interaction. This was realized, first by coupling the ηN and πN channels [1], and subsequently verified in works that generate dynamically the $N^*(1535)$ S_{11} resonance, e.g. Ref. [2], by considering the entire set of pseudoscalar meson–octet baryon coupled channels. It was soon suggested that η -nuclear quasibound states might exist [3, 4]. While various optical model calculations produce invariably such states across the periodic table, the value of mass number A that marks the

*corresponding author: Avraham Gal, avragal@savion.huji.ac.il

onset of binding depends on which underlying ηN interaction is chosen and on how its subthreshold energy dependence is handled [5, 6, 7, 8, 9]. For recent reviews, see Refs. [10, 11]. Yet, no such states have ever been established beyond doubt [12].

Electromagnetic and hadronic production reactions on nuclear targets provide useful constraints on the existence of η quasibound states in very light nuclei. The most recent interpretation of these data is that ηd is unbound, $\eta^3\text{He}$ is nearly or just bound, and $\eta^4\text{He}$ is bound [13]. Unfortunately, the η -nucleus optical model approach mentioned above is not trustable in these light nuclei, and genuine few-body calculations are required. Our previous few-body ηNN and ηNNN calculations agree with this conjecture as far as the ηd and $\eta^3\text{He}$ systems are concerned [14]. A similar conclusion for $\eta^3\text{He}$ has been reached recently by evaluating the $pd \rightarrow \eta^3\text{He}$ near-threshold reaction [15]. As for a possible $\eta^4\text{He}$ bound state, it has been searched upon with the WASA-at-COSY facility in the $dd \rightarrow ^3\text{He}N\pi$ reaction [16], placing upper limits of a few nb on the production of a bound $\eta^4\text{He}$.

On the theoretical side, precise ηNNN and $\eta NNNN$ stochastic variational method (SVM) bound-state calculations that use a $\not\pi$ EFT (pionless effective field theory) approach have just been published, coauthored by us [17]. These calculations suggest that the onset of η -meson binding in the ^3He nucleus requires that the real part of the ηN scattering length $a_{\eta N}$, $\text{Re} a_{\eta N}$, exceeds 1 fm approximately, yielding then a few MeV η binding in ^4He , and that the onset of η -meson binding in the ^4He nucleus requires that $\text{Re} a_{\eta N}$ exceeds 0.7 fm approximately. Another very recent work [18] reports on few-body calculations of the η - ^3He and η - ^4He scattering lengths, concluding that for $\text{Re} a_{\eta N} \approx 0.9$ fm neither $\eta^3\text{He}$ nor $\eta^4\text{He}$ are bound.

Here we extend the SVM few-body bound-state calculations of Ref. [17], replacing the $\not\pi$ EFT NN and NNN contact interactions used there by the same Minnesota [19] and Argonne AV4' [20] semi-realistic NN interactions used in our previous ηNN and ηNNN hyperspherical-basis calculations [14]. We confirm the results and conclusions of that work for ηNN and ηNNN . Our results compare well with those reached in the $\not\pi$ EFT approach [17].

The paper is organized as follows. The two-body NN and ηN input interactions are specified in Sect. 2 and the way we handle the subthreshold energy dependence of the input ηN interaction is described in Sect. 3. Results of our SVM calculations of ηNNN and $\eta NNNN$ quasibound states are given in Sect. 4 and compared in Sect. 5 with results of optical-model calculations. Finally, conclusions are drawn in Sect. 6.

2. Two-body interaction input

In this section we describe the choice of NN and ηN pairwise interactions.

2.1. NN potentials

Two forms of central NN potentials were used in the present work. These are denoted MNC for the Minnesota potential [19] and AV4p for the Argonne AV4' potential [20] parametrized in terms of Gaussians. These central potentials were also used in our previous work [14]. Both potentials produce nearly identical values of binding energy for the weakly bound deuteron, as seen in Table 1, but differ in the 1S_0 NN low-energy scattering parameters input which enters the calculation of the $A=3,4$ nuclei binding energies listed below. They also differ in their short-range repulsion which is much stronger in AV4p than in MNC. We note that the binding energy of ^3H within the present AV4' parametrization is smaller by 0.11 MeV than that used in our previous work [14]. The proton-proton Coulomb interaction is included in these calculations.

Table 1: Binding energies B (in MeV) of s -shell nuclei calculated by applying the SVM to the MNC [19] and AV4p [20] NN central potentials.

NN int.	$B(^2\text{H})$	$B(^3\text{H})$	$B(^4\text{He})$
MNC	2.202	8.380	29.90
AV4p	2.199	8.884	32.03
Exp.	2.225	8.482	28.30

2.2. ηN potentials

The ηN interaction has been studied in coupled-channel models that fit or generate dynamically the $N^*(1535)$ S_{11} resonance which peaks about 50 MeV above the ηN threshold. The resulting ηN scattering amplitudes exhibit substantial model dependence, as demonstrated in Fig. 1 where the real and imaginary parts of the ηN center-of-mass (cm) s -wave scattering amplitude $F_{\eta N}$ are plotted as a function of the cm energy \sqrt{s} for several coupled channel models. A feature in common to all these models is that both real and imaginary parts of $F_{\eta N}$ decrease monotonically upon going deeper into the subthreshold region. Focusing on the ηN scattering length $a_{\eta N}$, which stands

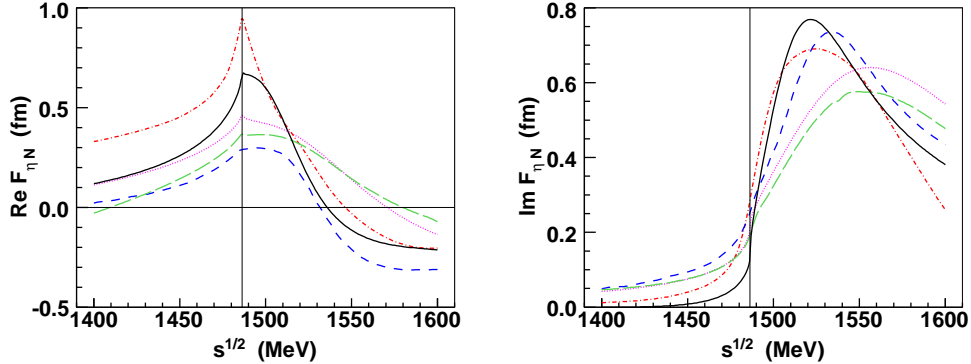


Figure 1: Real (left panel) and imaginary (right panel) parts of the ηN cm s -wave scattering amplitude $F_{\eta N}$ as a function of the total cm energy $s^{1/2}$ in five meson-baryon coupled-channel interaction models, in decreasing order of $\text{Re } a_{\eta N}$. Dot-dashed curves: GW [21]; solid: CS [22]; dotted: KSW [23]; long-dashed: M2 [24]; short-dashed: IOV [25]. The thin vertical line denotes the ηN threshold. Figure adapted from Ref. [10].

for the value the ηN scattering amplitude $F_{\eta N}$ at threshold, the figure exhibits a wide range of values for the real part $\text{Re } a_{\eta N}$ from 0.2 fm [2] to almost 1.0 fm [21]. The imaginary part $\text{Im } a_{\eta N}$, in contrast, is constrained by near-threshold data that involve mostly the coupling to the πN channel and hence displays a considerably narrower range of values, from 0.2 to 0.3 fm.

Our ηN potentials are derived from ηN s -wave scattering amplitudes $F_{\eta N}$ calculated in two of the meson-baryon coupled-channel interaction models, GW [21] and CS [22], shown in Fig. 1. Whereas the GW model which was considered in our previous work [14] is a K -matrix model that accounts for the coupling between the ηN and πN channels, the CS model is a genuine meson-baryon multi-channel model. The scattering length $a_{\eta N}$ is given in these two models by

$$a_{\eta N}^{\text{GW}} = (0.96 + i0.26) \text{ fm}, \quad a_{\eta N}^{\text{CS}} = (0.67 + i0.20) \text{ fm}. \quad (1)$$

Following a procedure introduced by Hyodo and Weise [26] for using effective $\bar{K} N$ potentials below threshold, we construct local but energy-dependent complex potentials $v_{\eta N}$ that generate the ηN s -wave scattering amplitude $F_{\eta N}$ below threshold in models GW and CS. This proved useful in K^- few-nucleon calculations [27, 28, 29] and in our previous work on η few-nucleon quasibound states [14]. Below we denote by $\delta\sqrt{s} \equiv \sqrt{s} - \sqrt{s_{\text{th}}}$ the energy

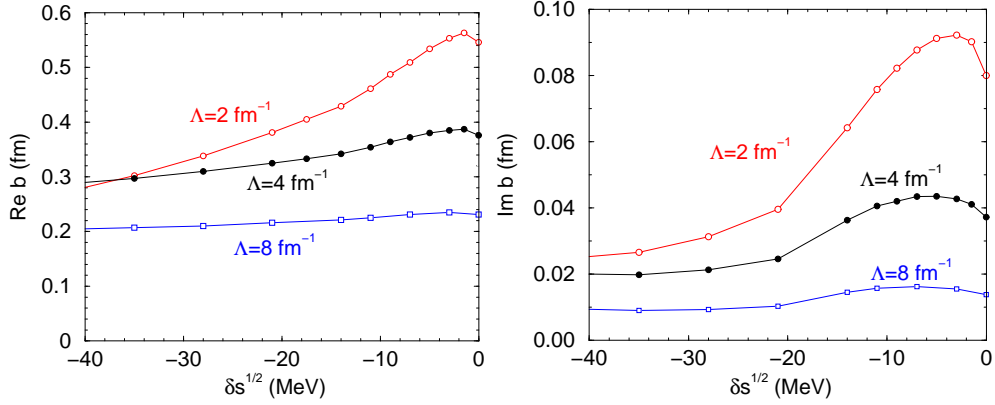


Figure 2: Real (left) and imaginary (right) parts of the strength function b of the ηN effective potential (2) at subthreshold energies, $\delta\sqrt{s} < 0$, for three values of the scale parameter Λ , as obtained from the scattering amplitude $F_{\eta N}^{\text{GW}}$ [21] shown in Fig. 1.

argument of $v_{\eta N}$ and of $F_{\eta N}$ with respect to the ηN threshold, with $\delta\sqrt{s} < 0$ for subthreshold energies. The form chosen for the ηN potential $v_{\eta N}$ is

$$v_{\eta N} = -\frac{4\pi}{2\mu_{\eta N}} b(\delta\sqrt{s}) \rho_{\Lambda}(r), \quad (2)$$

where $\mu_{\eta N}=346$ MeV is the reduced ηN mass, b is an energy dependent strength function, and $\rho_{\Lambda}(r)$ is a normalized Gaussian:

$$\rho_{\Lambda}(r) = \left(\frac{\Lambda}{2\sqrt{\pi}}\right)^3 \exp\left(-\frac{\Lambda^2 r^2}{4}\right), \quad (3)$$

with a scale parameter Λ inversely proportional to the range of $v_{\eta N}$. As argued in Ref. [26], Λ is related to the EFT momentum breakdown scale corresponding to vector-meson exchange: $\Lambda \lesssim m_{\rho} = 3.9 \text{ fm}^{-1}$. A more restrictive upper bound value of $\Lambda \lesssim 3.0 \text{ fm}^{-1}$ arises from excluding the ρN channel in dynamically generating the $N^*(1535)$ resonance [14]. Nevertheless, in order to study the scale dependence of our results, we temporarily disregard such constraints on Λ and consider here three representative values: $\Lambda=2,4,8 \text{ fm}^{-1}$, the latter corresponding to extremely short-ranged interaction.

For a given value of the scale parameter Λ , the subthreshold values of the complex strength function b of Eq. (2) were fitted, as detailed in Sect. 2.1 of Ref. [14], to the complex phase shifts derived from the corresponding values

of the subthreshold scattering amplitude $F_{\eta N}$. Such strength functions are shown in Fig. 2 for three values of the scale parameter Λ in model GW [21]. The curves for b exhibit monotonic decrease below threshold except for some Λ dependent humps near threshold that reflect, perhaps, the threshold cusp of $\text{Re } F_{\eta N}$ in Fig. 1. Nevertheless, the subthreshold values $\delta\sqrt{s}$ relevant for our calculations are all below -10 MeV and are unaffected by these humps. Similar curves for b are obtained in model CS, with values smaller uniformly for both real and imaginary parts than model GW yields, in accordance with the relative strength of the generating subthreshold scattering amplitudes $F_{\eta N}$ shown in Fig. 1. Finally we note that the decrease of b upon increasing Λ , say for $\text{Re } b$ at threshold, follows from the Λ independence of the generating $\text{Re } F_{\eta N}$; a Λ independent b would necessarily lead to ηN bound states for sufficiently large values of Λ .

3. Energy dependence

Here we outline the self consistent procedure adopted in our previous applications [14, 17] for coping with the energy dependent ηN effective potential $v_{\eta N}$ discussed in Sect. 2.2. One needs to determine the most appropriate *input* value $\delta\sqrt{s}$ of the subthreshold ηN energy at which $v_{\eta N}$ should enter the η -nuclear few-body calculation. To this end, following Ref. [29], an *average* ηN \sqrt{s}_{av} over the A bound nucleons is introduced by

$$A\sqrt{s}_{\text{av}} = \sum_{i=1}^A \sqrt{(E_{\eta} + E_i)^2 - (\vec{p}_{\eta} + \vec{p}_i)^2}. \quad (4)$$

Expanding about threshold, with $\sqrt{s}_{\text{th}} \equiv E_{\text{th}} = m_N + m_{\eta} = 1487$ MeV, one obtains

$$\sqrt{s}_{\text{av}} \approx \sqrt{s}_{\text{th}} - \frac{B}{A} + \frac{A-1}{A}E_{\eta} - \frac{1}{A} \sum_{i=1}^A (\vec{p}_{\eta} + \vec{p}_i)^2 / (2E_{\text{th}}), \quad (5)$$

where B is the total binding energy of the η -nuclear system. Transforming in the total cm system the momentum dependent part to kinetic energies and taking expectation values in the η -nuclear bound state, one obtains

$$\langle \delta\sqrt{s} \rangle = -\frac{B}{A} - \xi_N \frac{A-1}{A} \langle T_{N:N} \rangle + \frac{A-1}{A} \langle E_{\eta} \rangle - \xi_{\eta} \left(\frac{A-1}{A} \right)^2 \langle T_{\eta} \rangle, \quad (6)$$

where $\xi_{N(\eta)} \equiv m_{N(\eta)}/(m_N + m_\eta)$. Here, T_η is the η kinetic energy operator in the η -nucleus cm frame, $T_{N:N}$ is the pairwise NN kinetic energy operator in the NN pair cm frame and $E_\eta = (H - H_N)$, with the nuclear Hamiltonian H_N evaluated in its own cm frame and the total Hamiltonian H evaluated in the η -nucleus cm frame. We note that the imaginary part of the ηN interaction, discussed below in Sect. 4, was excluded from the present construction so that both B and $\langle E_\eta \rangle$ are real, with $B > 0$ and $\langle E_\eta \rangle < 0$ for η -nuclear bound states. Finally, for $A=1$ the last three terms on the r.h.s. of Eq. (6) vanish, leading to $\langle \delta\sqrt{s} \rangle_{\eta N} = -B$ as expected.

Since all terms on the r.h.s. are negative definite, the two-body energy argument $\delta\sqrt{s}$ of $v_{\eta N}$ that enters the few-body calculation forms a continuous distribution in the subthreshold region that is replaced in non-Faddeev few-body calculations [10] by the output expectation value $\langle \delta\sqrt{s} \rangle$. This expression was used in our 2015 calculations for $A = 2, 3$ employing hyperspherical basis expansion of η -nuclear wavefunctions [14]. Switching to SVM correlated Gaussian basis in our 2017 $\not\neq$ EFT calculations [17] as well as here, we found it more useful to rewrite Eq. (6) as

$$\langle \delta\sqrt{s} \rangle = -\frac{B}{A} - \xi_N \frac{1}{A} \langle T_N \rangle + \frac{A-1}{A} \langle E_\eta \rangle - \xi_A \xi_\eta \left(\frac{A-1}{A} \right)^2 \langle T_\eta \rangle, \quad (7)$$

where $\xi_A \equiv Am_N/(Am_N + m_\eta)$. Here, T_N and T_η are the nuclear and η kinetic energy operators evaluated in terms of internal Jacobi coordinates, with the total intrinsic kinetic energy of the system given by $T = T_N + T_\eta$. Since $(A-1)\langle T_{N:N} \rangle$ in Eq. (6) equals $\langle T_N \rangle$ here, Eq. (7) coincides with the former equation apart from a kinematical factor ξ_A introduced here to make correspondence with the η -nuclear, last Jacobi coordinate with which T_η is associated.

Requiring that the output expectation value $\langle \delta\sqrt{s} \rangle$ given by Eq. (7), as derived from the solution of the few-body Schroedinger equation, agrees with the input value $\delta\sqrt{s}$ for $v_{\eta N}$, this equation defines a self-consistency cycle in our few-body η -nuclear calculations. As argued above, the self consistent energy shift $\delta\sqrt{s_{sc}}$ is negative definite, with size exceeding a minimum nonzero value obtained from the first two terms in the limit of vanishing η binding. Eq. (7) in the limit $A \gg 1$ coincides with the nuclear-matter expression used in Refs. [8, 9] for calculating η -nuclear quasibound states.

The following two figures demonstrate how the self consistency requirement works in actual calculations. The curves plotted in Fig. 3 are obtained

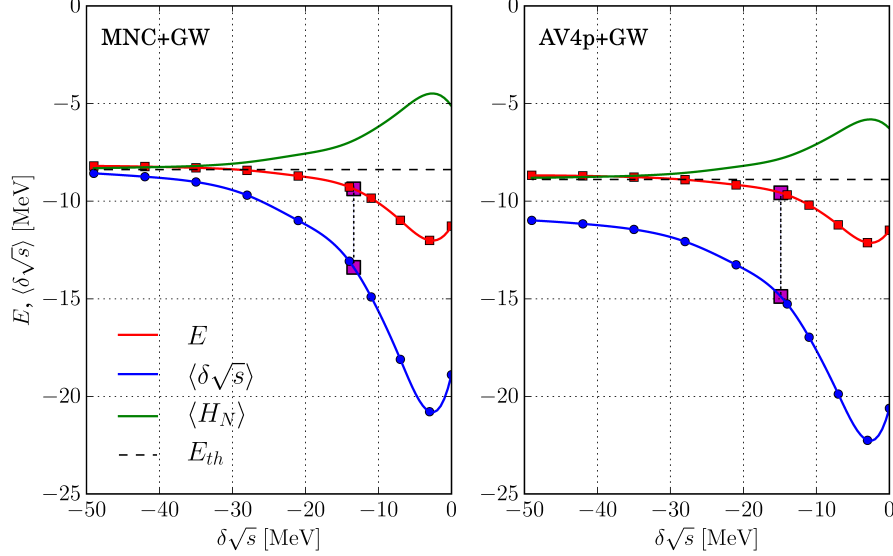


Figure 3: η ${}^3\text{H}$ bound-state energies E (squares) and expectation values $\langle\delta\sqrt{s}\rangle$ (circles) from Eq. (7), obtained in SVM calculations that use the MNC (left panel) and AV4p (right panel) NN potentials, as a function of the subthreshold energy input argument $\delta\sqrt{s}$ of $v_{\eta N}^{\text{GW}}$ for $\Lambda = 4 \text{ fm}^{-1}$. The dashed vertical line marks the self consistent output values of E and $\langle\delta\sqrt{s}\rangle$. The dashed horizontal line marks the ${}^3\text{H}$ core g.s. energy serving as threshold for a bound η , and the curve above it shows the squeezed core energy $\langle H_N \rangle$.

by interpolating a sequence of calculated η ${}^3\text{H}$ bound-state energies (squares) and the corresponding expectation values $\langle\delta\sqrt{s}\rangle$ (circles) from Eq. (7) for $A = 3$, as a function of the input energy argument $\delta\sqrt{s}$ of $v_{\eta N}^{\text{GW}}$ with a momentum scale parameter $\Lambda = 4 \text{ fm}^{-1}$ and using the NN potential MNC (left panel) and AV4p (right panel). The dashed vertical line marks the self consistent value of $\delta\sqrt{s}$ at which the outcome bound-state energy $E(\eta$ ${}^3\text{H})$ is evaluated. Both lower and middle curves are located, as they should, *below* the dashed horizontal line that marks the ${}^3\text{H}$ core bound-state energy which serves as threshold energy for the η ${}^3\text{H}$ bound state. In contrast, the upper curve which shows the expectation value $\langle H_N \rangle$ of the nuclear core energy is located *above* this dashed horizontal line. Finally, we note that the η binding (or more precisely separation) energy B_η is about 1.0 MeV in the left panel (MNC) and 0.7 MeV in the right one (AV4p), a few MeV less than what a $v_{\eta N}$ fitted exclusively to $F_{\eta N}$ at threshold yields. The somewhat weaker η

binding for AV4p with respect to that for MNC is related to the considerably stronger short-range repulsive component present in the NN potential AV4p. Although computed for $\eta^3\text{H}$, these B_η values agree to within 15 ± 10 keV with those that were checked in a sample $\eta^3\text{He}$ calculation, so from here on we shall treat them as $\eta^3\text{He}$ results. These B_η values are also consistent with those calculated by us previously [14].

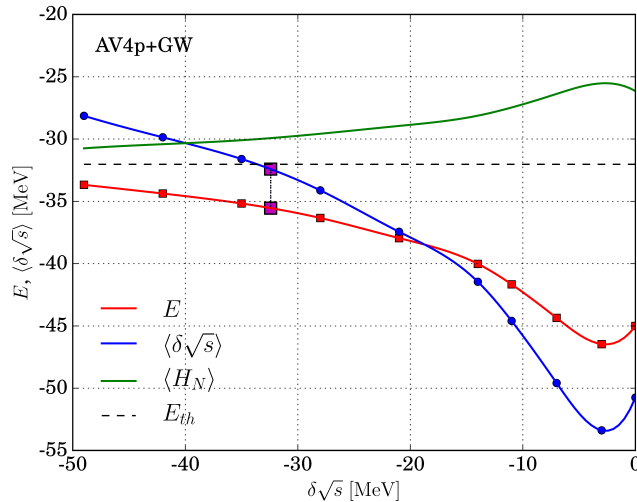


Figure 4: Same as in Fig. 3, but for $\eta^4\text{He}$ using the AV4p NN potential.

Fig. 4 for $\eta^4\text{He}$ is similar to Fig. 3 (right) for $\eta^3\text{H}$, using the AV4p NN potential. The self consistent value of B_η , about 3.5 MeV, is larger here than the 0.7 MeV there; however it is much smaller, almost by 10 MeV, than what a threshold $v_{\eta N}$ yields, owing to the subthreshold energy dependence of $v_{\eta N}$. Note that the self consistent value $\delta\sqrt{s_{sc}}$ in the compact ^4He core (about -32 MeV, see Fig. 4) is considerably farther away from threshold than its counterpart in ^3H (about -15 MeV, see Fig. 3, right).

4. Results

The present few-body self consistent stochastic-variational-method (SVM) calculations follow those of Ref. [17] where this method is briefly discussed. Our results for $\eta^3\text{He}$ bound states are listed in Table 2 and shown in Fig. 5,

and for η ⁴He in Table 3 and Fig. 6, for several choices of $(NN, \eta N)$ potential combinations, each one for three values of the momentum scale parameter Λ . Along with η binding (separation) energies B_η and widths Γ_η , we also list the self consistent values $\delta\sqrt{s_{sc}}$ at which these values of B_η and Γ_η were evaluated, plus expectation values of potential and kinetic energies. Noting that $\text{Im } b \ll \text{Re } b$, see Fig. 2, the binding energies B_η were evaluated using real Hamiltonians in which $\text{Im } v_{\eta N}$ was neglected, and the η -nuclear widths Γ_η were calculated perturbatively using wavefunctions $\Psi_{\text{g.s.}}$ generated by these real Hamiltonians, viz.

$$\Gamma_\eta = -2 \langle \Psi_{\text{g.s.}} | \text{Im } V_\eta | \Psi_{\text{g.s.}} \rangle . \quad (8)$$

Here, V_η sums over all pairwise ηN interactions. Since $|\text{Im } V_\eta| \ll |\text{Re } V_\eta|$, this is a reasonable approximation. Restoring $\text{Im } V_\eta$, it was estimated, by solving the corresponding optical-model η -nucleus bound-state equation with and without $\text{Im } V_\eta$, that B_η decreases by less than 0.3 MeV for weakly bound states.

Table 2: η ³He bound state energies, widths and shifts (in MeV) from SVM calculations using 3 values of Λ (in fm⁻¹) for several choices of $(NN, \eta N)$ pairwise potentials. The listed values of Γ_η outdate the excessively large widths listed in Ref. [14] that arose from a programming error. The number of displayed digits reflects the numerical accuracy of these calculations.

Λ	$\delta\sqrt{s_{sc}}$	$\langle V_N \rangle$	$\langle T_N \rangle$	$\langle V_\eta \rangle$	$\langle T_\eta \rangle$	B_η	Γ_η
		<i>NN: MNC</i>		<i>ηN: GW</i>			
2	-9.385	-36.636	28.384	-3.376	3.148	0.099	1.144
4	-13.392	-39.655	32.767	-15.002	12.520	0.990	3.252
8	-18.787	-40.983	37.534	-30.956	24.592	1.433	3.280
		<i>NN: AV4p</i>		<i>ηN: GW</i>			
2	-11.478	-47.599	38.805	-2.365	2.304	-0.028	0.769
4	-14.881	-51.199	43.383	-11.885	10.131	0.686	2.438
8	-18.234	-52.182	46.438	-21.981	17.891	0.950	2.332
		<i>NN: MNC</i>		<i>ηN: CS</i>			
2	-8.388	-35.600	27.243	-0.251	0.446	-0.217	0.057
4	-8.712	-35.931	27.657	-1.312	1.367	-0.161	0.227
8	-9.402	-36.263	28.352	-3.509	3.145	-0.105	0.385

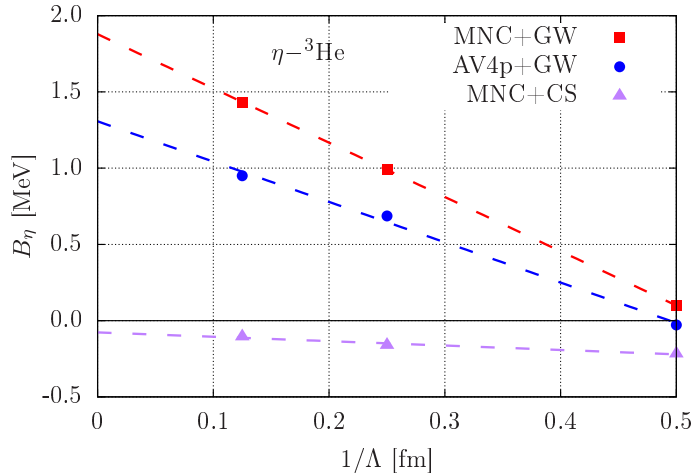


Figure 5: $B_\eta(\eta^3\text{He})$ values from Table 2 as a function of $1/\Lambda$, calculated within several combinations of $(NN, \eta N)$ potentials marked in the upper-right corner.

The tables demonstrate that the smaller the range ($\sim 1/\Lambda$) of the ηN interaction, the larger is the resulting η binding energy B_η , in spite of the increased value of $-\delta\sqrt{s_{sc}}$ which implies a weaker ηN potential strength b . In fact, all of the entities listed in these tables increase in magnitude with Λ , particularly $\langle V_\eta \rangle$ and $\langle T_\eta \rangle$ once the η -nuclear system becomes bound. Nevertheless, the η averaged momentum encountered there reaches a modest maximal value of $\langle p_\eta^2 \rangle^{\frac{1}{2}} = 1.08 \text{ fm}^{-1}$, for (MNC, GW) with $\Lambda = 8 \text{ fm}^{-1}$ in $\eta^4\text{He}$, in spite of the much larger momenta that this scale parameter is capable of generating. For a given ηN potential, here GW, more binding is obtained with the MNC NN potential than with the more realistic AV4p, as already noted in the discussion of Fig. 3. And finally, for a given NN potential, here MNC, more binding is obtained obviously using GW than the weaker CS for the ηN potential. In fact CS does not bind $\eta^3\text{He}$, as indicated by the negative values for B_η listed in the last group in Table 2 and as shown by the lower curve in Fig. 5. These results are consistent with those in Ref. [14]. For $\eta^4\text{He}$, although Table 3 and Fig. 6 suggest that a bound state exists for the combination $(NN:\text{MNC}, \eta N:\text{CS})$, it is doubtful whether CS can really bind $\eta^4\text{He}$ for the more realistic AV4p NN interaction.

Figs. 5 and 6 suggest a significant theoretical uncertainty in the computed η binding energies B_η for two reasons. First, for a given choice of NN and ηN

Table 3: SVM calculations of η ^4He bound states, see caption of Table 2 for details.

Λ	$\delta\sqrt{s_{\text{sc}}}$	$\langle V_N \rangle$	$\langle T_N \rangle$	$\langle V_\eta \rangle$	$\langle T_\eta \rangle$	B_η	Γ_η
		<i>NN</i> : MNC		ηN : GW			
2	-19.477	-90.052	60.330	-8.783	7.645	0.96	1.975
4	-29.750	-95.510	68.527	-32.925	25.320	4.69	4.500
8	-43.294	-97.754	78.466	-65.387	47.982	6.79	6.196
		<i>NN</i> : AV4p		ηN : GW			
2	-23.646	-120.760	88.965	-6.356	5.744	0.38	1.207
4	-32.411	-127.922	97.998	-26.851	21.233	3.51	3.615
8	-40.279	-129.720	104.085	-46.116	34.994	4.71	4.198
		<i>NN</i> : MNC		ηN : CS			
2	-16.704	-88.149	58.239	-0.938	1.107	-0.16	0.133
4	-19.246	-89.948	60.566	-8.468	7.483	0.47	0.901
8	-22.434	-90.942	63.210	-17.007	14.021	0.82	1.108

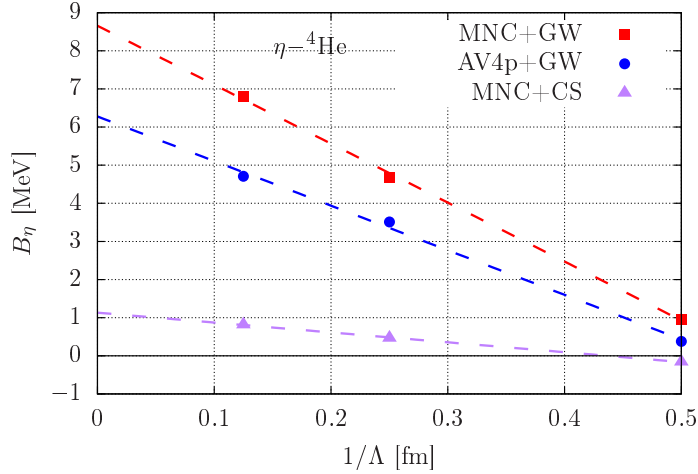


Figure 6: $B_\eta(\eta^4\text{He})$ values from Table 3 as a function of $1/\Lambda$, calculated within several combinations of (NN , ηN) potentials marked in the upper-right corner.

interaction models, say the (AV4p, GW) combination, the computed values of B_η depend on the scale parameter Λ of the Gaussian shape assumed for $v_{\eta N}$. As stated above, the smaller the range ($\sim 1/\Lambda$) of the ηN interaction,

the larger B_η is, consistently with the observation made long ago for B_Λ in Λ hypernuclear few-body calculations [30]. In our previous work [14] we argued that $\Lambda \lesssim 3 \text{ fm}^{-1}$ holds implicitly in the $N^*(1535)$ resonance meson-baryon models within which the ηN scattering amplitude $F_{\eta N}$ is determined. Excluding therefore as high values as $\Lambda = 8 \text{ fm}^{-1}$, this would mean that the GW ηN interaction binds both He isotopes, with $B_\eta(\eta^3\text{He})$ about 0.3 MeV or less and $B_\eta(\eta^4\text{He}) \lesssim 2 \text{ MeV}$ upon using the more realistic AV4p NN interaction. The second origin of theoretical uncertainty concerns the choice of ηN interaction model: choosing CS instead of the GW interaction, for example, one could envisage an unbound $\eta^3\text{He}$ and a very slightly bound $\eta^4\text{He}$. Finally, if the ηN interaction is weaker than CS, it is likely that neither $\eta^3\text{He}$ nor $\eta^4\text{He}$ are bound. In the next section we discuss, for comparison, optical-model calculations of $\eta^3\text{He}$ and $\eta^4\text{He}$ bound states.

5. Comparison with other model calculations

In this section we connect between the few-body η -nuclear calculations pursued in the main part of the present work and optical-model approaches applied to heavier nuclei, normally for $A \geq 12$, as summarized by Mareš et al. [11]. In particular, Xie et al. [15] recently fitted the strongly energy dependent $dp \rightarrow \eta^3\text{He}$ cross sections near threshold using a ‘ $t_{\eta N} \rho_A$ ’ optical model approach, where $t_{\eta N}$ is directly related to the ηN scattering length $a_{\eta N}$ and ρ_A is the nuclear g.s. static density normalized in coordinate space to A . These authors derived an effective value

$$a_{\eta N}^{\text{eff}} = [(0.48 \pm 0.05) + i(0.18 \pm 0.02)] \text{ fm}, \quad (9)$$

claiming that although insufficient to generate a bound state pole, nevertheless it generates a virtual-state pole near threshold corresponding to $B_\eta \approx -0.3 \text{ MeV}$ and $\Gamma \approx 3.0 \text{ MeV}$. This effective value $a_{\eta N}^{\text{eff}}$ is necessarily smaller than the value of the scattering length $a_{\eta N}$ owing to the reduction that both values of $\text{Re } F_{\eta N}$ and $\text{Im } F_{\eta N}$ undergo below threshold. The actual value of $a_{\eta N}$ in their model could well come close to that of $a_{\eta N}^{\text{CS}}$, Eq. (1). It is interesting then to see whether the larger values in models GW and CS of $\text{Re } a_{\eta N}$ compared to the ‘effective’ values cited in Eq. (9) are able to generate $\eta^3\text{He}$ and $\eta^4\text{He}$ bound states in this optical model approach.

Within the underlying Watson (W) multiple scattering series [32], the $t\rho$

optical potential in momentum space assumes the form

$$\tilde{V}_{\eta A}^{\text{W}}(q) = -\frac{4\pi}{2\mu_{\eta N}} \mathcal{F}_{\eta N}(q) \tilde{\rho}_A(q), \quad (10)$$

where the ηN subthreshold energy dependence is implicit. A Gaussian momentum dependence was adopted for both the cm scattering amplitude $\mathcal{F}_{\eta N}$ and the momentum-space nuclear density $\tilde{\rho}_A$:

$$\mathcal{F}_{\eta N}(q) = F_{\eta N} \exp\left(-\frac{q^2}{\Lambda^2}\right), \quad \tilde{\rho}_A(q) = A \exp\left(-\frac{q^2}{\lambda_A^2}\right), \quad (11)$$

with Λ chosen the same as in the Gaussian form (2) of $v_{\eta N}$. Fourier transforming the product $\mathcal{F}_{\eta N}(q) \times \tilde{\rho}_A(q)$ to coordinate space, we obtain

$$\exp\left(-\frac{q^2}{\Lambda^2}\right) \tilde{\rho}_A(q) \Rightarrow A(R_A \sqrt{\pi})^{-3} \exp\left(-\frac{r^2}{R_A^2}\right), \quad R_A^2 = r_0^2 + r_A^2, \quad (12)$$

with $r_0 = 2/\Lambda$ and $r_A = 2/\lambda_A$, where $r_3 = 1.436$ fm and $r_4 = 1.165$ fm are the Gaussian size parameters of the point-nucleon density distributions of ${}^3\text{He}$ and ${}^4\text{He}$, respectively, derived by unfolding the proton charge distribution from the nuclear charge distribution [31]. Finally, to incorporate the leading $1/A$ correction, we go to the KMT form of the optical potential [33], as applied e.g. by Feshbach et al. [34], multiplying the Watson optical potential (10) by $(A-1)/A$.¹ Hence:

$$V_{\eta A}^{\text{KMT}}(r) = -\frac{4\pi}{2\mu_{\eta N}} F_{\eta N} (A-1) (R_A \sqrt{\pi})^{-3} \exp\left(-\frac{r^2}{R_A^2}\right). \quad (13)$$

In Table 4 we list η binding energies and widths calculated in the He isotopes using the optical potential (13) for ηN scale parameter $\Lambda = 4$ fm⁻¹ and with the GW and CS scattering amplitudes $F_{\eta N}$ evaluated at both threshold energy $\delta\sqrt{s} = 0$, and at the subthreshold energies $\delta\sqrt{s_{\text{sc}}}$ found in the few-body self consistent calculations listed in Tables 2 and 3 for $(NN, \eta N)$ potential combinations (AV4p, GW) and (MNC, CS). The results show that of

¹This $(A-1)/A$ factor takes care of the antisymmetrization of nucleons in intermediate multiple-scattering states. To get the meson-nuclear overall T matrix, one then multiplies the T matrix arising from V^{KMT} by $A/(A-1)$; see Sect. 4.2 in Ref. [32] for a detailed exposition.

Table 4: $1s_\eta$ binding energies B_η and widths Γ_η (in MeV) calculated for $\eta^3\text{He}$ and $\eta^4\text{He}$ by using the KMT η -nuclear optical potential (13) for ηN scale parameter $\Lambda = 4 \text{ fm}^{-1}$ and with scattering amplitudes $F_{\eta N}^{\text{GW}}$ and $F_{\eta N}^{\text{CS}}$, each evaluated at threshold $\delta\sqrt{s} = 0$ and also at self-consistent subthreshold energies $\delta\sqrt{s_{\text{sc}}}$ (in MeV) listed in Sect. 4. Results from the present few-body (FB) calculations, with AV4p along with GW and MNC along with CS, and from those in Ref. [17] are also listed.

ηN model	η -nuclear model	$\eta^3\text{He}$			$\eta^4\text{He}$		
		$\delta\sqrt{s}$	B_η	Γ_η	$\delta\sqrt{s}$	B_η	Γ_η
GW [21]	optical	0	0.33	6.04	0	25.1	40.8
	FB (present)	0	2.60	5.08	0	13.0	12.0
	FB [17]	0	3.62	7.52	0	10.8	13.2
	optical	-14.9	-	-	-32.4	1.03	2.35
	FB (present)	-14.9	0.69	2.44	-32.4	3.51	3.62
	FB [17]	-21.1	0.30	1.46	-32.2	1.54	2.82
CS [22]	optical	0	-	-	0	6.39	21.0
	FB (present)	0	0.30	2.16	0	6.77	11.3
	FB [17]	0	-	-	0	3.47	8.95
	optical	-8.7	-	-	-19.2	-	-
	FB (present)	-8.7	-	-	-19.2	0.47	0.90
	FB [17]	-9.9	-	-	-23.7	-	-

the four cases studied within the optical-model approach $\eta^3\text{He}$ is bound, and quite slightly so, only by choosing the scattering amplitude $F_{\eta N}^{\text{GW}}$ at threshold to work with. Once a self consistent value $\delta\sqrt{s_{\text{sc}}}$ is used to represent the ηN subthreshold energy appropriate in a few-body $\eta N N N$ calculation, the slight $\eta^3\text{He}$ binding shown in the first row of the table disappears. The ηN CS scattering amplitude does not produce binding at all, in agreement with the $\eta^3\text{He}$ few-body calculations listed in Table 2. For $\eta^4\text{He}$ both optical-model strengths at threshold produce substantial values of B_η and particularly of Γ_η . Here too, consideration of the appropriate subthreshold energy reduces these values, leaving $\eta^4\text{He}$ weakly bound only for the GW choice of ηN interaction. Finally, the table also demonstrates good agreement between the present SVM results and those obtained in recent $\not\equiv$ EFT SVM calculations.

6. Conclusion

In conclusion, we have presented truly few-body SVM calculations of ηNNN ($\eta^3\text{He}$) and $\eta NNNN$ ($\eta^4\text{He}$) bound states, using semi-realistic NN interactions and ηN subthreshold interactions derived in coupled channels studies of the $N^*(1535)$ nucleon resonance. Considering ηN scale parameters $\Lambda = 2, 4 \text{ fm}^{-1}$, while excluding as high value as $\Lambda = 8 \text{ fm}^{-1} \gg m_\rho$ which corresponds to extremely short-ranged interaction, the present results suggest that the onset of $\eta^3\text{He}$ binding occurs for $\text{Re } a_{\eta N}$ close to 1 fm, as in model GW [21], consistently with our previous hyperspherical-basis ηNNN calculations [14]. The onset of $\eta^4\text{He}$ binding requires a lower value of $\text{Re } a_{\eta N}$ around 0.7 fm which is comfortably satisfied in model GW and almost in model CS [22]. These results are also in good agreement with the very recent SVM calculations coauthored by us [17] which use a $\not\propto$ EFT approach. Further dedicated experimental searches for $\eta^4\text{He}$ bound states are needed in order to confirm the recent negative report from COSY [16] which, taken at face value, implies that $\text{Re } a_{\eta N} \lesssim 0.7 \text{ fm}$.

We have also compared our few-body calculations with leading-order optical model calculations that use the same subthreshold energies $\delta\sqrt{s}$ as those determined self consistently in the few-body calculations. Careful attention was paid to $1/A$ corrections. These optical model calculations, which produce less binding than that produced in the corresponding few-body calculations, nevertheless give *qualitatively* similar results to those of the few-body calculations. Ignoring the energy dependence of the input ηN amplitude leads to strongly excessive binding energies, and widths, in both approaches.

Acknowledgments

We thank Jiří Mareš and Martin Schaefer for helpful discussions on related matters, and Eulogio Oset and Colin Wilkin for helpful exchanges on the contents of Ref. [15]. This work was supported in part (NB) by the Israel Science Foundation grant 1308/16 and by PAZI Fund grants, and in part (EF, AG) by the EU initiative FP7, Hadron-Physics3, under the SPHERE and LEANNIS cooperation programs.

References

- [1] R.S. Bhalerao, L.C. Liu, Phys. Rev. Lett. 54 (1985) 865.

- [2] N. Kaiser, T. Waas, W. Weise, Nucl. Phys. A 612 (1997) 297, and references to earlier work cited therein.
- [3] Q. Haider, L.C. Liu, Phys. Lett. B 172 (1986) 257.
- [4] L.C. Liu, Q. Haider, Phys. Rev. C 34 (1986) 1845.
- [5] Q. Haider, L.C. Liu, Phys. Rev. C 66 (2002) 045208.
- [6] C. García-Recio, T. Inoue, J. Nieves, E. Oset, Phys. Lett. B 550 (2002) 47.
- [7] D. Jido, H. Nagahiro, S. Hirenzaki, Phys. Rev. C 66 (2002) 045202.
- [8] E. Friedman, A. Gal, J. Mareš, Phys. Lett. B 725 (2013) 334.
- [9] A. Cieplý, E. Friedman, A. Gal, J. Mareš, Nucl. Phys. A 925 (2014) 126.
- [10] A. Gal, E. Friedman, N. Barnea, A. Cieplý, J. Mareš, D. Gazda, Acta Phys. Polon. B 45 (2014) 673.
- [11] J. Mareš, N. Barnea, A. Cieplý, E. Friedman, A. Gal, EPJ Web of Conf. 130 (2016) 03006.
- [12] C. Wilkin, EPJ Web of Conf. 130 (2016) 01007.
- [13] B. Krusche, C. Wilkin, Prog. Part. Nucl. Phys. 80 (2015) 43.
- [14] N. Barnea, E. Friedman, A. Gal, Phys. Lett. B 747 (2015) 345.
- [15] J.J. Xie, W.H. Liang, E. Oset, P. Moskal, M. Skurzok, C. Wilkin, Phys. Rev. C 95 (2017) 015202.
- [16] P. Adlarson, et al. (WASA-at-COSY Collaboration), Nucl. Phys. A 959 (2017) 102.
- [17] N. Barnea, B. Bazak, E. Friedman, A. Gal, Phys. Lett. B 771 (2017) 297.
- [18] A. Fix, O. Kolesnikov, Phys. Lett. B 772 (2017) 663.
- [19] D.R. Thompson, M. LeMere, Y.C. Tang, Nucl. Phys. A 286 (1977) 53.
- [20] R.B. Wiringa, S.C. Pieper, Phys. Rev. Lett. 89 (2002) 182501.

- [21] A.M. Green, S. Wycech, Phys. Rev. C 71 (2005) 014001.
- [22] A. Cieplý, J. Smejkal, Nucl. Phys. A 919 (2013) 46.
- [23] N. Kaiser, P.B. Siegel, W. Weise, Phys. Lett. B 362 (1995) 23.
- [24] M. Mai, P.C. Bruns, U.-G. Meißner, Phys. Rev. D 86 (2012) 094033.
- [25] T. Inoue, E. Oset, M.J. Vicente Vacas, Phys. Rev. C 65 (2002) 035204.
- [26] T. Hyodo, W. Weise, Phys. Rev. C 77 (2008) 035204.
- [27] A. Doté, T. Hyodo, W. Weise, Nucl. Phys. A 804 (2008) 197.
- [28] A. Doté, T. Hyodo, W. Weise, Phys. Rev. C 79 (2009) 014003.
- [29] N. Barnea, A. Gal, E.Z. Liverts, Phys. Lett. B 712 (2012) 132.
- [30] B.F. Gibson, D.R. Lehman, Phys. Rev. C 23 (1981) 404.
- [31] I. Angeli, K.P. Marinova, At. Data and Nucl. Data Tables 99 (2013) 69.
- [32] J.M. Eisenberg, D.S. Koltun, *Theory of Meson Interactions with Nuclei* (Wiley, New York, 1980) ISBN 0-471-03915-2.
- [33] A.K. Kerman, H. McManus, R.M. Thaler, Ann. Phys. 8 (1959) 551, reprinted in 281 (2000) 853.
- [34] H. Feshbach, A. Gal, J. Hüfner, Ann. Phys. 66 (1971) 20.